Journal of Environmental Chemical Engineering 6 (2018) 197–207

Contents lists available at ScienceDirect

Journal of Environmental Chemical Engineering

journal homepage: www.elsevier.com/locate/jece

Photocatalysis with easily recoverable linear engineered TiO_2 nanomaterials to prevent the formation of disinfection byproducts in drinking water

Stephanie L. Gora[a,*], Robert Liang[b], Y. Norman Zhou[b], Susan A. Andrews[a]

[a] Department of Civil Engineering, University of Toronto, 35 St. George Street, Toronto, Ontario, M5S 1A4, Canada
[b] Department of Mechanical and Mechatronics Engineering, University of Waterloo, 200 University Avenue West, Waterloo, Ontario, N2L 3G1, Canada

ARTICLE INFO

Keywords:
Photocatalysis
Engineered nanomaterials
Disinfection byproducts
Drinking water treatment
AOP
Natural organic matter

ABSTRACT

Two photocatalytic linear engineered TiO_2 nanomaterials (LENs) were synthesized and evaluated against commercial standard P25 TiO_2 nanoparticles in terms of their effects on common parameters used to measure and characterize natural organic matter (NOM) and disinfection byproduct (DBP) precursors in drinking water. DBPs, some of which have been linked to cancer and other negative human health outcomes, are regulated in most jurisdictions in North America and Europe as well as parts of Asia, Africa, and South America, and the removal of DBP precursors is a central goal of conventional drinking water treatment plants. All three of the nanomaterials evaluated in this study were capable of degrading NOM, including DBP precursors, when irradiated with UVA LED light. The materials differed in terms of crystal phase, surface morphology, and available surface area. These differences impacted the predominant NOM removal processes occurring in each case and consequently the overall treatment efficacy of the two materials in two different water sources. One of the LENs evaluated in this study, designated NB 700, reduced the DBP formation potential of one of the water sources by 90% and was readily removed from the water via filtration. Irrespective of the nanomaterial employed, DBP precursor degradation was faster in the water source with higher NOM and lower alkalinity and hardness. The electrical energy per order (EEO) required to degrade DOC and THM precursors in one of the water sources was comparable to reported values for the degradation of these compounds with UV/H_2O_2, another advanced oxidation process.

1. Introduction

The removal of natural organic matter (NOM) is one of the primary goals of modern drinking water treatment plants because it can interfere with many standard drinking water treatment processes and reacts with chlorine and other chemical disinfectants to form an array of regulated and unregulated disinfection byproducts (DBPs). Recent research suggests that although commonly regulated classes of DBPs such as trihalomethanes (THMs) and haloacetic acids (HAAs) are less of a concern for human health than unregulated DBPs [1], their presence after chlorination has nonetheless been shown to be a good predictor of DBP formation in general [2]. Preventing the formation of DBPs by removing their precursor compounds (i.e. NOM) ahead of chlorination has become a common practice in drinking water treatment plants. Coagulation with metal salts has traditionally been the primary treatment method used for NOM removal in conventional water treatment plants. More recently, adsorption, high pressure membrane filtration, and various oxidative strategies such as ozonation and advanced oxidation processes, have also been employed for the removal of DBP precursors. In this study, we evaluated photocatalysis with linear engineered titanium dioxide (TiO_2) nanomaterials illuminated by UVA LEDs as an alternative to these existing processes. It has been established that TiO_2 photocatalysis degrades NOM and that it preferentially targets large and aromatic NOM compounds [3,4]. The effect of TiO_2 photocatalysis on DBP formation is less clear cut – a few studies have noted decreases in DBP formation potential (DBPfp), but others have observed increased DBPfp as larger molecules are broken down into smaller, more reactive ones [3,5–8]. Increases in DBPfp appear to be related to experimental design, in particular, irradiation time or UV dose (fluence). Studies focusing on short irradiation times have often

Abbreviations: AOP, Advanced oxidation process; DBP, Disinfection byproduct; DBPfp, Disinfection byproduct formation potential; DOC, Dissolved organic carbon; EEO, Electrical energy per order; HAA, Haloacetic acid; HAAfp, Haloacetic acid formation potential; LEN, Linear engineered nanomaterial; NOM, Natural organic matter; ROS, Reactive oxygen species; SUVA, Specific UV absorbance at 254 nm; THM, Trihalomethane; THMfp, Trihalomethane formation potential; UV254, UV absorbance at 254 nm; UVA, Ultraviolet light between 315 and 400 nm

* Corresponding author.
E-mail addresses: stephanie.gora@mail.utoronto.ca (S.L. Gora), rliang@uwaterloo.ca (R. Liang), nzhou@uwaterloo.ca (Y.N. Zhou), sandrews@civ.utoronto.ca (S.A. Andrews).

https://doi.org/10.1016/j.jece.2017.11.068
Received 5 October 2017; Received in revised form 17 November 2017; Accepted 25 November 2017
Available online 26 November 2017
2213-3437/ © 2017 Elsevier Ltd. All rights reserved.

noted increases in DBPfp [7] whereas those employing longer irradiation have usually reported decreases [3].

The characteristics of the background water matrix are known to affect the degradation rates of target compounds. NOM itself is frequently cited as the most important inhibitor of degradation in studies focused on the photocatalytic removal of more common organic indicators and pollutants [9]. Many inorganic components of natural water also have effects, both positive and negative, on the adsorption and degradation of target compounds by TiO_2. Turbidity, which disperses light, and some organic compounds that absorb UVA wavelengths can reduce the amount of useable light that reaches the photocatalyst. Chloride and bicarbonate are known scavengers of hydroxyl radicals [10], one of the main reactive oxygen species (ROS) formed during photocatalysis, while other ions such as phosphate and sulphate can bind to adsorption sites on the surface of the photocatalyst [11,12]. Higher ion levels can lead to a reduction in the electrostatic repulsive forces between individual nanoparticles, resulting in agglomeration [13–15], and a decrease in available surface area, which is likely to affect the extent of adsorption and photocatalysis. The effects of some inorganic parameters are more complex. For example, although the presence of calcium ions increases NOM adsorption to TiO_2 [14,16], it also encourages TiO_2 nanomaterials to agglomerate, even in the presence of NOM [15], and as such may indirectly slow degradation by decreasing the total available surface area. Iron readily adsorbs to TiO_2 [17] and both copper and iron can promote faster reactions between TiO_2 and organic contaminants [18,19]. Many of the effects described above are pH dependent and some parameters can interact with one another as well as with NOM and TiO_2, making it difficult to predict the overall effect of a given matrix on the rate of photocatalytic degradation.

Common issues preventing the use of suspended TiO_2 in an aqueous medium include the provision of adequate mixing, the distribution of light within the medium, and the removal of the photocatalyst after treatment. Much research has been conducted to engineer TiO_2 materials that are easier to remove from water, usually by immobilizing standard anatase or P25 nanoparticles on solid supports. This has proven challenging, though a few researchers have had success with magnetic TiO_2 nanomaterials [20] and TiO_2-covered zeolites [21]. TiO_2-based linear engineered nanomaterials (LENs) including nanotubes, nanowires, and nanobelts have been synthesized and characterized by research groups around the world in recent years. These materials are mainly used in sensors and solar cells [22], but may also prove to be useful in drinking water applications. Specifically, previous research has demonstrated that TiO_2 -based LENs can adsorb and degrade NOM [14,23,24], and their large size relative to standard nanoparticles may make them easier to remove via common drinking water clarification processes such as filtration or sedimentation [24].

LENs can be synthesized via alkaline hydrothermal, anodic, or template-guided sol-gel methods. The alkaline hydrothermal method is well established, does not require highly specialized laboratory equipment or expensive reagents, and is easily manipulated to yield nanosize materials with different morphological and chemical characteristics [22]. Survey studies have established that the precursor materials, hydrothermal synthesis temperature, extent and method of post synthesis cleaning and ion exchange, and calcination temperature have important effects on the final products of the synthesis process [25–29].

This study evaluated the photocatalytic degradation of NOM in two Canadian surface waters by three TiO_2 nanomaterials: P25 nanoparticles and two LENs synthesized in our laboratory. The calcination temperature used in the final step of the LEN synthesis process was varied in order to manipulate the crystal phase structure and surface properties of the LENs. The main objective of the study was to evaluate the effects of these LEN properties on the eventual formation of DBPs after photocatalytic treatment and subsequent chlorination. To the authors' knowledge, no other research groups have conducted work linking the synthesis conditions of LENs to the degradation of DBP precursors in drinking water.

2. Materials and methods

2.1. Materials

Evonik Degussa P25 TiO_2 nanoparticles were used as the reference material for all experiments and as the precursor material for the two LENs. All remaining reagents were obtained from Sigma Aldrich. Raw water was obtained from two Canadian water treatment plants (WTPs) supplied by river water sources. The Otonabee River (OTB), located in Southern Ontario, supplies the City of Peterborough while the Ottawa River (OTW) supplies the Britannia WTP, one of the two major WTPs that serve the City of Ottawa. Raw water samples were taken at the inlet of each water treatment plant ahead of prechlorination and used without further modification. A water quality summary is provided in Table 1. Both water sources had historical pH values near 8 and dissolved organic carbon (DOC) levels ranging from approximately 4–6 mg/L. The UV absorbance at 254 nm (UV254), an indicator of the amount of aromatic carbon present in a water sample, was nearly twice as high in the OTW water as in the OTB water. The OTW water's specific UV absorbance (SUVA) value, an indicator of the overall aromaticity of the NOM present in the water, was 3.7 ± 0.3 m/mg L compared to 2.6 ± 0.4 m/mg L in the OTB water, indicating that the NOM in the OTW water was more aromatic in character than that in the OTB water. The water sources also differed in terms of turbidity, alkalinity, calcium content, and conductivity (an indicator of ionic strength), many of which can affect degradation rates [10–12], NOM adsorption to TiO_2 [14,30,31], and/or the stability of nanomaterial suspensions. [14,32–34]. The OTB water had higher alkalinity, a higher overall concentration of ions, and approximately four times as much calcium as the OTW water while the OTW water contained higher concentrations of iron and copper relative to the OTB water.

2.2. Apparatus

The UVA LED apparatus used in this study consisted of four UVA lamps secured to a stand above a multiple location stir plate that was able to accommodate four beakers at once. A schematic of the experimental apparatus is provided in Fig. 1. The UVA LEDs (LZ1 UV 365 nm Gen2 Emitter, LED Engin Inc.) had a maximum irradiance at 365 nm. The average irradiance across the surface of the sample was calculated using a spreadsheet developed by Bolton and Linden [36] and was determined to be 4.9 mW/cm^2. The irradiance of each lamp was

Table 1
Summary of raw water quality.

Parameter	Units	Otonabee River (OTB)	Ottawa River (OTW)
DOC[a]	mg/L	4.7 ± 0.2	6.2 ± 0.5
UV254[a]	1/cm	0.120 ± 0.015	0.234 ± 0.030
SUVA[a]	L/mg.m	2.6 ± 0.4	3.7 ± 0.3
pH[b]		8.2 ± 0.2	7.7 ± 0.2
Turbidity[b]	NTU	0.6 ± 0.2	3.3 ± 1.0
Alkalinity[b]	mg/L as $CaCO_3$	87 ± 7	28 ± 6
Hardness[b]	mg/L as $CaCO_3$	95 ± 11	30 ± 6
Calcium[b]	mg/L	32.8 ± 3.7	8.3 ± 1.5
Magnesium[b]	mg/L	3.2 ± 0.3	2.2 ± 0.4
Sodium[b]	mg/L	6.5 ± 0.8	3.4 ± 0.8
Chloride[b]	mg/L	11.5 ± 1.3	3.3 ± 0.9
Conductivity[b]	µS/cm	214 ± 19	81 ± 13
Aluminum	µg/L	3.9 ± 1.8	165 ± 47
Copper	µg/L	0.7 ± 0.1	27 ± 10
Iron[b]	µg/L	19 ± 9	217 ± 42
Manganese[b]	µg/L	10 ± 6	11 ± 4

[a] Average and standard deviation of samples analyzed in the laboratory.
[b] Average and standard deviation of values obtained from Ontario Drinking Water Surveillance Program 2010–2012 [35].

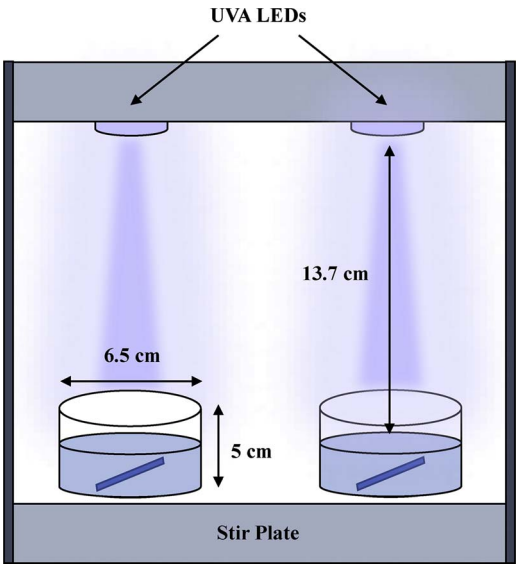

Fig. 1. Experimental UVA LED apparatus used in NOM degradation experiments.

confirmed before each test using a radiometer (International Light, ILT1400) equipped with a sensor optimized to measure light at 365 nm (International Light, XRL140B).

2.3. Synthesis and characterization of engineered TiO_2 nanomaterials

Two linear TiO_2 nanomaterials were synthesized from P25 nanoparticles according to a simple hydrothermal method first used by Kasuga et al. [37] and later modified by others including Yuan and Su [25]. Both materials were synthesized at 240 °C and then calcined at 550 °C (NB 550) or 700 °C (NB 700). They were then rinsed twice with distilled water to remove unreacted material and/or smaller linear particles, thus insuring a more consistent final product.

Each batch of LENs was evaluated using a quality control test to assess batch to batch consistency. Triplicate samples containing 50 mL of 0.03 M methylene blue solutions dosed with 0.1 g/L of TiO_2 were irradiated with UVA light (365 nm) with an average irradiance of 4.9 mW/cm^2 for 30 min. After irradiation, the TiO_2 was removed from the samples via centrifugation and the absorbance of the remaining solution at 665 nm was analyzed and used to calculate the concentration of methylene blue remaining in solution. On average, NB 550 achieved 53% methylene blue removal and NB 700 achieved 89% methylene blue removal. Batches that came within 5% of the average methylene blue removal were kept and used for experiments.

The LENs were characterized using transmission electron microscopy (TEM) to observe shape and surface characteristics, selected area electron diffraction (SAED) to determine crystal phase, zeta potential at different pH values to identify the isoelectric point, and N_2 adsorption isotherms to obtain surface area. TEM and SAED observation was conducted using a JEOL 2010F TEM/STEM at the Canadian Centre for Electron Microscopy (Hamilton, Ontario, Canada). The images were processed using Gatan Microscopy Suite: Digial Micrograph™ and SAED and FFT images were indexed using CrysTBox – diffractGUI [38]. N_2 adsorption isotherms were measured with a Quantachrome AUTOSORB-1. The samples were outgassed at 200 °C under vacuum for 12 h before the measurement. Surface area was determined by applying Brunauer–Emmett–Teller (BET) adsorption method on N_2 adsorption isotherms in a relative pressure range of 0.05–0.25.

The isolectric point (IEP) of the LENs was determined by measuring the zeta potential of 0.1 g/L TiO_2 solutions prepared in 10 mM NaCl and adjusted to pHs ranging from 3 to 9. The pH at which the zeta potential reached 0 was designated the IEP of the material. All samples were prepared in triplicate and the zeta analyzer made four measurements of each sample.

The formation of hydroxyl radicals by P25 and the two LENs was investigated using a simple fluorescence-based method [39,40]. Triplicate 50 mL samples of 0.5 mM TPA in 6 mM of NaOH were dosed with 0.02 g/L of TiO_2 and exposed to UVA LED light for 0, 0.5, 1, 2, 5, and 10 min, corresponding to approximate UV doses (fluences) of 0–4.4 J/cm^2 and approximate power per volume values of 0 to 13.5 kWh/m^3. The treated samples were filtered through a 0.45 µm polyethersulfone (PES) filter to remove the TiO_2 from solution and analyzed for the presence of HTPA. Previous research has suggested that approximately 80% of the total hydroxyl radicals present in solution will react with TPA to form HTPA [41], and thus the concentration of HTPA in the treated solution can be assumed to be a conservative low estimate of the total number of hydroxyl radicals formed during the photocatalytic treatment. Light only control samples were prepared irradiating the TPA solution with UVA light for 15 min. No evidence of HTPA formation was observed in these controls.

2.4. Filtration

A standard bench top filtration apparatus equipped with a PES lab filter with a pore size of 0.8 µm was used to test the filterability of the three nanomaterials using a modified version of the time to filter test (Standard Methods 2710-H [42]). The apparatus was connected to a vacuum pump set to provide 34 kPa (4.9 psi) of pressure on the permeate side of the filter. Each PES filter was flushed with 100 mL of purified water before being used to filter a 50 mL sample. The flux of purified water under these conditions was 6.8 m/h, which is within the 5 to 15 m/h range expected for granular media filters in drinking water treatment plants [43]. Filtration samples were prepared with 0.25 g/L of TiO_2 and mixed in the dark for 1 min ahead of filtration. The time required to filter each sample was recorded and normalized to the amount of time required to filter 50 mL of distilled water through the apparatus to yield a filtration index value. All filtration experiments were conducted in triplicate. The results of these simplified separation and filtration tests cannot be used to predict the long term behaviour of full-scale media or membrane filters, however, they do provide some indication of the relative filterability of the LENs used in this study.

2.5. NOM degradation experiments

All degradation experiments were conducted in continuously mixed batch reactors filled with 50 mL of untreated OTB or OTW water. The reactors were dosed with 0.25 g/L of TiO_2 and exposed to the UVA LEDs for 0, 5, 15, 30, 45, or 60 min, corresponding to UV doses of 0 to 17.6 J/cm^2 and power per volume of 0 to 54 kWh/m^3. The treated river water samples were filtered through a 0.45 µm PES filter to remove the TiO_2 nanomaterials and analyzed for UV254, DOC, chlorine demand, trihalomethane formation potential (THMfp), and haloacetic acid formation potential (HAAfp). Chlorine demand, THMfp, and HAAfp were assessed at uniform formation conditions (UFC) as described by Summers et al. [44]. The THMs and HAAs formed during this process were extracted according to Standard Method 6232 B and Standard Method 6251 B [42] and analyzed using an Agilent 7890 B GC-ECD. All NOM removal experiments were conducted in quadruplicate with one replicate being used for chlorine demand and three being used for DBPfp determination.

2.6. Calculations

Electrical energy per order (EEO) is generally reported in units of kWh/order/m^3 and refers to the electrical energy required to reduce the concentration of a contaminant to one tenth its original value in 1 m^3 of water. It is currently listed as a “figure of merit” for the evaluation of advanced oxidation processes by the International Union of Pure and Applied Chemistry (IUPAC). The EEO of a given process can be

Table 2
Shape size, and surface characteristics of P25 nanoparticles and lab synthesized LENs.

Material	P25	NB 550	NB 700
Shape	Spherical	Linear	Linear
Diameter	21 nm[a]	–	–
Length	–	0.5–2 μm	0.5–2 μm
Width	–	20–200 nm	20–200 nm
Surface Characteristics	–	Speckled	Smooth
Predominant Crystal Phase	Anatase and Rutile	Anatase and TiO_2 (B)	Anatase
BET Surface Area	57 m^2/g	30 m^2/g	18 m^2/g
Isoelectric Point (IEP)	pH 6 to 6.5	pH 4 to 4.5	pH 4 to 4.5
Apparent k_{OH}[b]	0.62 ± 0.03 mM/min	0.10 ± 0.01 mM/min	0.74 ± 0.06 mM/min
Apparent k_{OH} (normalized)[c]	10.9 ± 0.5 mM/min/m^2	3.5 ± 0.3 mM/min/m^2	41.4 ± 3.2 mM/min/m^2

[a] Sigma Aldrich.
[b] Apparent zero order reaction rate constant.
[c] Apparent zero order reaction rate constant normalized to available photocatalyst surface area.

calculated using Eq. (1), where P is the power dissipated by the treatment process (kW), V is the volume of water treated in the experiment (L), C_i is the original concentration of the contaminant, C_f is the final concentration of the contaminant, and t is the time required to achieve C_f (min).

$$EEO = \frac{1000Pt}{V\log\left(\frac{C_i}{C_f}\right)} \quad (1)$$

All statistical analyses were conducted at the 95% confidence level.

3. Results

3.1. Characterization of engineered TiO_2 nanomaterials

The LENs in this study were characterized in terms of size (TEM), crystal phase structure (SAED), isoelectric point (zeta potential), surface area (BET isotherm testing), and hydroxyl radical production. The results are summarized in Table 2. The temperature setpoints used during the LEN synthesis process had important effects on many of these parameters. These have been discussed in the context of previous research on TiO_2-based LENs.

Survey studies [25–27] have established that the precursor materials, hydrothermal synthesis temperature, extent and method of post synthesis cleaning and ion exchange, and calcination temperature have important effects on the final products. The choice of precursor materials and hydrothermal temperature affects the overall size and aspect ratio of the linear nanomaterials, with higher temperatures generally resulting in larger materials [25]. The washing, ion exchange, and calcination steps affect the surface and crystalline structures of the materials, and thus their photocatalytic properties [27–29].

The TEM images of the LENs in Fig. 2 show that both nanomaterials were roughly rectangular or belt-like in shape. Individual belts ranged from 20 nm to 200 nm in width and from 500 nm to multiple microns in length. The LENs differed in terms of their surface topography. The NB 700 particles were smooth and the edges appeared rounded while the NB 550 particles appeared speckled with raised bumps and had sharply defined edges. Zheng et al. [28] reported similar surface characteristics for LENs calcined at similar temperatures and attributed them to the presence of different phases of TiO_2, namely anatase and TiO_2(B).

Anatase is widely held to be the most photoactive form of TiO_2 but some researchers have, however, reported that mixed phase anatase/TiO_2(B) LENs can be even more effective than pure anatase materials [28]. The predominant crystal phases present in the two LENs in the current study were determined using SAED and TEM analysis. The SAED images of NB 550 (Fig. 2A_1) reveal that NB 550 contained predominantly anatase, however, the TEM image (Fig. 2A_2) indicated that TiO_2(B) crystalline grains were also present with d-spacing of 0.36 nm and 0.57 nm corresponding to the (011) and (10-1) planes, respectively. The anatase grains indicate d-spacings for 0.34 nm and 0.38 nm, corresponding to the (101) and (003) planes of anatase. The interface between anatase and TiO_2(B) phases had similar lattice parameters. The (101) planes in anatase and (011) planes in TiO_2(B) also matched closely. When the calcination temperature increased to 700 °C, the TiO_2(B) was converted to anatase as shown in Fig. 2B. The d-spacings of NB 700 (Fig. 2B_2) were 0.35 nm and 0.45 nm, which match the (101) and (002) planes of anatase.

BET isotherm analysis showed that both LENs had less surface area than P25 nanoparticles (30 m^2/g and 18 m^2/g vs. 57 m^2/g). The higher surface area observed for the LENs calcined at 550 °C compared to those calcined at 700 °C is consistent with previous studies [27–29]. In theory, nanomaterials with higher surface area should be more effective for contaminant adsorption.

The isoelectric points (IEPs) of the LENs occurred at pH values between 4 and 4.5, which is below that of P25 (6 to 6.5). Previous work has established that the pH of the water has a strong effect on NOM adsorption to P25 and that adsorption is favoured when pH of the water is below the IEP the nanomaterial [4,30]. The implication of this finding is that the LENs will be negatively charged within the pH range commonly found in natural surface water sources (6.5–8.5) and thus may repel negatively charged water constituents, thus slowing or preventing their degradation. The IEPs of the nanomaterials may also have had an impact on the degree to which they agglomerated in each water source. Nanoparticle agglomeration and its effect on surface area can also contribute to the changes in adsorption efficiency and photocatalytic degradation observed at different pHs and in the presence of ions and NOM. Nanomaterial agglomeration and subsequent decrease in the overall available surface area is most likely to occur when the pH is near the isoelectric point/point of zero charge because at this pH repulsive forces between individual particles are at a minimum [14].

P25 and the two LENs were also evaluated in terms of hydroxyl radical production as described in Section 2.3. As shown in Fig. 3, P25 and NB 700 produced more hydroxyl radicals than NB 550. On a mole basis, the results of the current study are comparable to those of other researchers using similar, though not identical, experimental conditions [40]. The relationship between HTPA formation and time was linear in the range observed in this study, suggesting a zero order reaction between TPA and ·OH. This matches the findings of the study from which the experimental conditions for the current experiment were drawn [39]. The superior hydroxyl radical production of NB 700 relative to the other two materials was reflected in the reaction rate constants (k_{OH}) of the three nanomaterials, which are summarized in Table 2. The k_{OH} for NB 700 was 0.74 ± 0.06 mM/min, which was slightly but significantly higher than that of P25, which was 0.62 ± 0.03 mM/min, at the 95% confidence level. NB 550 lagged behind the other two materials with a k_{OH} of only 0.10 ± 0.01 mM/min. NB 700's superior hydroxyl radical

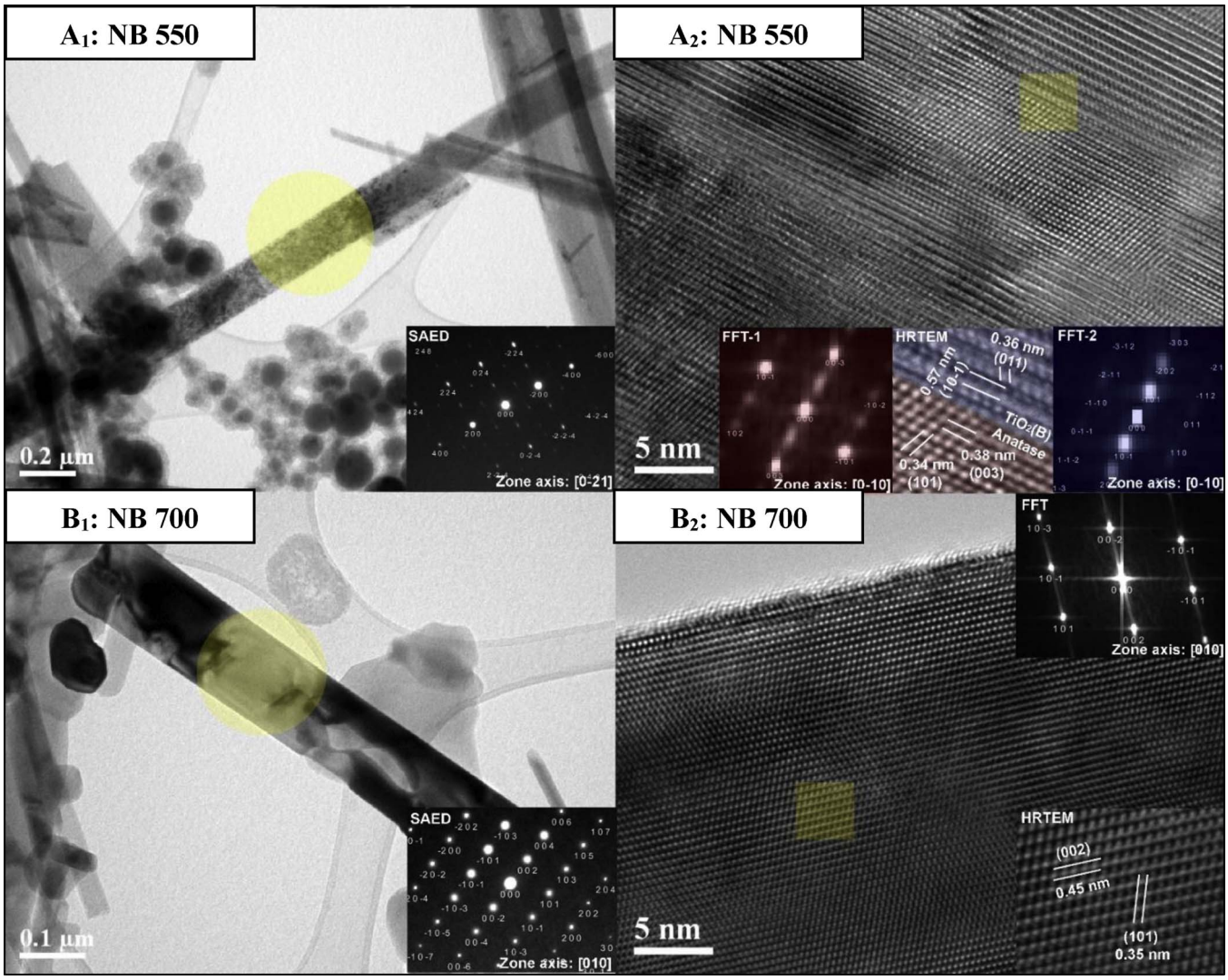

Fig. 2. Characterization of NB 550 (A) and NB 700 (B) via TEM and SAED.

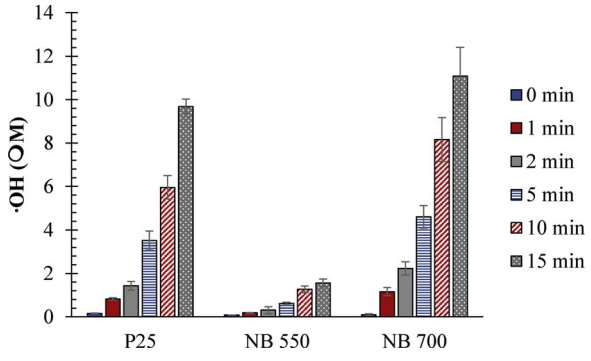

Fig. 3. Hydroxyl radical production by P25, NB 550, and NB 700 under UVA LED irradiation.

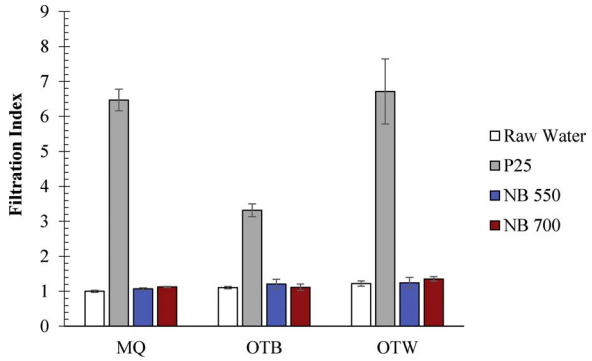

Fig. 4. Filtration indexes of 0.25 g/L suspensions of P25 nanoparticles, NB 550, and NB 700 in purified (MQ) water, Otonabee River (OTB) water, and Ottawa River (OTW) water.

production relative to P25 and NB 550 was further confirmed by the normalized reaction rate constants for the three materials, which are also shown in Table 2. The normalized k_{OH} for NB 700 was 41.4 ± 3.2 mM/min/m^2 while that of P25 was 10.9 ± 0.5 mM/min/m^2, indicating that NB 700 produced nearly four times as many moles of HTPA, and thus ·OH radicals, per unit area as P25.

3.2. Filtration

Filtration is commonly used to separate TiO_2 from water in bench-scale experiments and is a promising separation option for full-scale water treatment with TiO_2 nanomaterials. Fig. 4 shows the filtration index of each raw water and water containing 0.25 g/L of the three nanomaterials. The filtration indexes of the two raw river water

samples were nearly equal to 1, indicating that they did not present a significant barrier to filtration relative to distilled water. The OTW water had a slightly higher filtration index (1.22 ± 0.07) than the OTB water (1.11 ± 0.04), likely owing to its higher turbidity and organic content. The raw water flux values for OTB and OTW water were 6.1 m/h and 5.5 m/h respectively, which is within the accepted range for granular media filtration (5 m/h–15 m/h) but well above that achieved by microfiltration membranes (0.03 m/h–0.17 m/h).

Irrespective of the water matrix used, water flowed through the lab filter more quickly when the water contained NB 550 or NB 700 rather than P25 nanoparticles (Fig. 4). In fact, in the tests conducted with the two natural water samples there was no statistical difference at the 95% confidence level between the filtration indexes of the raw water samples and those of the water samples containing NB 550 or NB 700. The LENs were larger than the membrane pores in at least one dimension, and as such, may have been more likely to be retained on the surface of the membrane during filtration than the much smaller P25 nanoparticles, which may have been more likely to enter and clog the pores of the membrane. Indeed, the samples containing P25 had filtration indexes three to six times greater than those containing the LENs. This is in agreement with the findings of Zhang et al. [23], who used membrane filtration to separate P25 nanoparticles and two LENs from water. Based on the results of membrane fouling tests and SEM imaging, they hypothesized that the P25 nanoparticles were becoming lodged in the pores of the membrane during filtration, constricting them and increasing the resistance to flow while the LENs formed a looser, more porous cake on the membrane surface that had less of an effect on flow. The experimental results of the current study suggest that similar phenomena occurred in this case and clearly demonstrate the superior filterability of the LENs relative to standard P25 nanoparticles in purified water and both surface water matrices.

The filtration index of the P25 suspension in OTB water was approximately half that of the P25 suspension in OTW water (3.32 ± 0.18 vs. 6.71 ± 0.93), indicating that the P25 nanoparticles were more easily removed from the OTB water matrix than from the OTW water matrix. This was likely because the nanoparticles formed larger agglomerates in the former than in the latter. Nanoparticle agglomeration, a complex phenomenon that is influenced by the composition of the water matrix as well as by the chemical and physical properties of the nanomaterial in question [14,15,32–34], was not explored in detail in this study, however, the results presented in Fig. 4 are in line with those of other researchers who have observed that nanoparticles are more likely to agglomerate in water with high ionic strength and less likely to do so in the presence of NOM (e.g. [14]).

3.3. Degradation of natural organic matter (dissolved organic carbon and UV254)

NOM (measured as DOC and UV254) was adsorbed and degraded by all three TiO_2 nanomaterials (Fig. 5). During the photocatalytic portion of the treatment UV254 decreased more quickly than DOC regardless of the TiO_2 material used. This difference in behaviour may indicate some preference for aromatic NOM but is also a function of the parameters themselves: DOC captures all of the original NOM compounds along with the intermediate organic products of their degradation whereas UV254 measures only that portion of NOM that contains aromatic or unsaturated structures. These structures are easier for ROS such as ·OH to disrupt and as such are the first to be broken, leading to an overall decrease in UV254.

NB 550 was less effective for DOC and UV254 removal than P25 nanoparticles or NB 700. The NB 700 was particularly effective and achieved 100% removal of both UV254 and DOC from the OTW water within 60 min of irradiation, indicating that all of the oxidizable NOM present in the sample had been mineralized. Decreases in both DOC and UV254 occurred more slowly in the OTB water than in the OTW water, likely because the former contained higher levels of known ROS

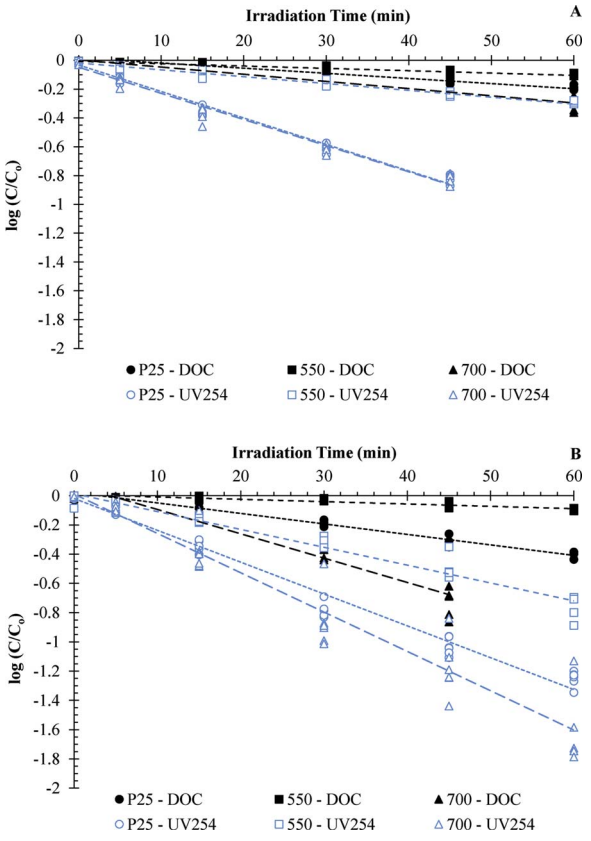

Fig. 5. Degradation of DOC and UV254 from (A) Otonabee River water and (B) Ottawa River water (B) by P25 nanoparticles, NB 550, and NB 700.

scavengers including chloride (11.5 ± 1.3 mg/L vs. 3.3 ± 0.9 mg/L) and bicarbonate (87 ± 7 mg/L as $CaCO_3$ vs. 28 ± 6 mg/L as $CaCO_3$). Alternatively or additionally, the presence of higher concentrations of Ca^{2+} and other ions in the OTB water compared to the OTW water (e.g. conductivity of OTB water = 214 ± 19 µS/cm, conductivity of OTW water = 81 ± 13 µS/cm) may have led to an increased degree of aggregation accompanied by an overall decrease in available surface area in this water source. Finally, as suggested by its higher SUVA value (3.7 ± 0.3 L/m.mg vs. 2.6 ± 0.4 L/m.mg), the OTW NOM was more aromatic in nature than the OTB NOM and as such may have been more vulnerable to oxidation, as has been observed by other researchers [3,8]. The degradation kinetics of DOC and UV254 were good fits to a simple pseudo-first order degradation model. The DOC and UV254 degradation rate constants for P25 and NB 700 were higher than those for NB 550 (Table 3) confirming that NOM degradation by P25 and NB 700 proceeded more quickly than for NB 550. The normalized degradation rate constants indicate that NB 700 was far more effective for DOC and UV254 on a per surface area basis than P25 or NB 550.

Adsorption played a minor but notable role in NOM removal in this study. P25 removed 14 ± 5% of the DOC and 30 ± 2% of the UV254 from the OTB water and 17 ± 6% of the DOC and 20 ± 3% of the UV254 from the OTW water. The LENs adsorbed less NOM; both removed approximately 6% of DOC and 10% of UV254 from both water sources. The superior adsorptive ability of the P25 nanoparticles is partly explained by available surface area: the BET surface area of the P25 nanoparticles was 57 m^2/g while those of NB 550 and NB 700 were 30 m^2/g and 18 m^2/g, respectively. Indeed, when DOC removal was normalized to surface area both P25 and NB 700 removed 0.08 mg DOC/m^2 from OTW water via adsorption (Table S.1). The surface-area-normalized reaction rate constants, which are also included in Table 3, suggest even more strongly that the superior NOM degradation ability of NB 700 relative to P25 was due to its ability to harness light to

Table 3
Apparent first order reaction rate constants and normalized reaction rate constants for DOC and UV254 removal.

	DOC			UV254		
	k min^{-1}	k norm $min^{-1}\,m^{-2}$	R^2	K min^{-1}	k norm $min^{-1}\,m^{-2}$	R^2
OTB						
P25	−0.004 ± 0.000	−0.005 ± 0.001	0.94	−0.018 ± 0.001	−0.026 ± 0.002	0.96
NB 550	−0.002 ± 0.000	−0.004 ± 0.001	0.88	−0.005 ± 0.000	−0.013 ± 0.001	0.96
NB 700	−0.005 ± 0.001	−0.024 ± 0.002	0.97	−0.018 ± 0.002	−0.080 ± 0.008	0.97
OTW						
P25	−0.008 ± 0.001	−0.011 ± 0.001	0.93	−0.022 ± 0.001	−0.031 ± 0.002	0.98
NB 550	−0.002 ± 0.000	−0.004 ± 0.001	0.88	−0.012 ± 0.001	−0.032 ± 0.004	0.94
NB 700	−0.017 ± 0.003	−0.074 ± 0.015	0.93	−0.027 ± 0.002	−0.120 ± 0.008	0.97

generate hydroxyl radicals.

In this study, the main energy input to the experimental apparatus was the UVA LEDs used to illuminate the samples. Each LED had a rated power demand of 2.7 W. This, along with the sample volume (50 mL), the time of irradiation (60 min), and the concentration of DOC measured in the raw and treated samples, was inputted into Eq. (1) (see Section 2.4) to determine the EEO of each material. EEO values for DOC removal by the three nanomaterials ranged from 37 kWh/order/m^3 for NB 700 in OTW water to over 500 kWh/order/m^3 for NB 550 in both water matrices. EEO values were higher in OTB, which contained a higher concentration of ROS scavengers, than OTW water. Yen and Yen [45] reported an EEO of 30 kWh/order/m^3 for DOC degradation by a UV/H_2O_2 system employing a low pressure UV lamp (maximum irradiance at 254 nm) and a 10 mg/L dose of H_2O_2. This is close to the EEO value calculated for NB 700 in the OTW water, suggesting that a UV/TiO_2 system employing NB 700 and UVA LED light might prove to be competitive with UV/H_2O_2 under certain experimental conditions and in some water matrices.

3.4. Removal and degradation of disinfection byproduct precursors

In this study, the total THMfp of both the OTB water and the OTW water initially increased when the samples were exposed to the UVA LEDs irrespective of the TiO_2 nanomaterial used before eventually decreasing at longer irradiation times (Fig. 6). The rate and extent of this increase was not constant: THMfp peaked between 5 and 15 min of irradiation depending on the nanomaterial and water matrix used. The initial increase in THMfp observed upon irradiation was likely related to the formation of reactive intermediates during the photocatalytic degradation process [4,8]. As irradiation time was increased, these reactive intermediates would themselves have been broken down by the photocatalytic degradation process, resulting in decreased THMfp. Liu et al. [8] noted a similar trend in one of the two Australian surface waters they treated with commercial P25 nanoparticles and UV light. They hypothesized that at short irradiation times larger NOM molecules were partially broken down such that more reactive sites became available for chlorine attack, resulting in increased THM formation upon chlorination. This phenomenon likely also contributed to increased THMfp at short irradiation times in the current study.All of the nanomaterials tested exhibited the initial peak followed by eventual THMfp reduction, but the rates and end points of the THMfp increases and decreases were different, suggesting that the three materials may have interacted with different components or to different extents with the raw water NOM. THMfp change was also water matrix specific. The THMfp of the treated OTB water was unchanged or above that of the raw OTB water after 60 min of irradiation with all three materials but that of the treated OTW water was well below that of the raw OTW water or that observed at shorter treatment times in this water matrix. One material, NB 700, reduced the THMfp of the OTW water by 92 ± 6% after 60 min of irradiation.

In this work, THMfp refers to the sum of four trihalomethane species commonly formed when NOM from surface water interacts with chlorine. Trichloromethane (TCM) and bromodichloromethane (BDCM) were the predominant THMs formed upon chlorination of the raw and treated water samples. Fig. 6 shows how the relative concentrations of TCM and BDCM changed over time in the treated samples. In general, the concentration of TCM decreased continuously with increasing irradiation time but at shorter irradiation times this reduction was accompanied by a gradual increase in BDCM. As the treatment proceeded, the BDCM precursors were eventually degraded, contributing to the reduction of overall THMfp. This is similar to results presented by Gerrity et al. [46], who explored the degradation of THM precursors in real surface water sources using a pilot scale UV/TiO_2 system.

All three TiO_2 nanomaterials reduced the THMfp of OTW water (Fig. 6D–F) more effectively than that of the OTB water (Fig. 6A–C). As was noted for DOC and UV254, factors that may explain this discrepancy include the higher concentrations of ROS scavengers such as bicarbonate in the OTB water; reduction in available surface area due to higher levels of agglomeration driven by a decrease in electrostatic repulsion in the ion-rich OTB water; increased NOM oxidation in the OTW water related to the presence of higher concentrations of iron and copper in this matrix (Table 1); and the characteristics of the NOM, including THM precursors, in each water source. As demonstrated in the hydroxyl radical production experiments described in Section 3.1 and Fig. 3, NB 700 was particularly effective for hydroxyl radical production. As such, its oxidative efficacy may have been more likely to be impacted by the presence of hydroxyl radical scavengers than that of the other nanomaterials, which removed NOM predominantly via other oxidative or adsorptive pathways.

Adsorption was less effective for THM precursor removal than it was for DOC and UV254 removal. Adsorption with P25 nanoparticles reduced the THMfp of the OTW water by 28 ± 9% while adsorption with NB 550 reduced the THMfp of the OTB water by 9 ± 6%. None of the other material/water matrix combinations resulted in statistically significant removal of THM precursors via adsorption.

Strictly speaking, the EEO concept assumes first order degradation kinetics and in most cases in this study, THMfp removal did not follow a first order reaction model. The exceptions were P25 and NB 700 in the OTW water, and this only after the peak that occurred between 5 and 15 min of irradiation. The EEO value for THMfp reduction by UVA/TiO_2 treatment with NB 700 in the OTW water (51 kWh/order/m^3) was comparable to that which has been reported for UV/H_2O_2 treatment with 10 mg/L of H_2O_2 (44 kWh/order/m^3) [45], indicating that under some conditions and with some TiO_2 materials UV/TiO_2 may prove to be competitive with UV/H_2O_2 for THMfp reduction. This should be confirmed by comparing the two processes under a variety of experimental conditions and in the same water matrices.

For the most part, the HAAfp results, shown in Fig. 7, followed the same trends as the THMfp results. Like THMfp, the term HAAfp refers to the likelihood that a water sample will form a suite of haloacetic acids

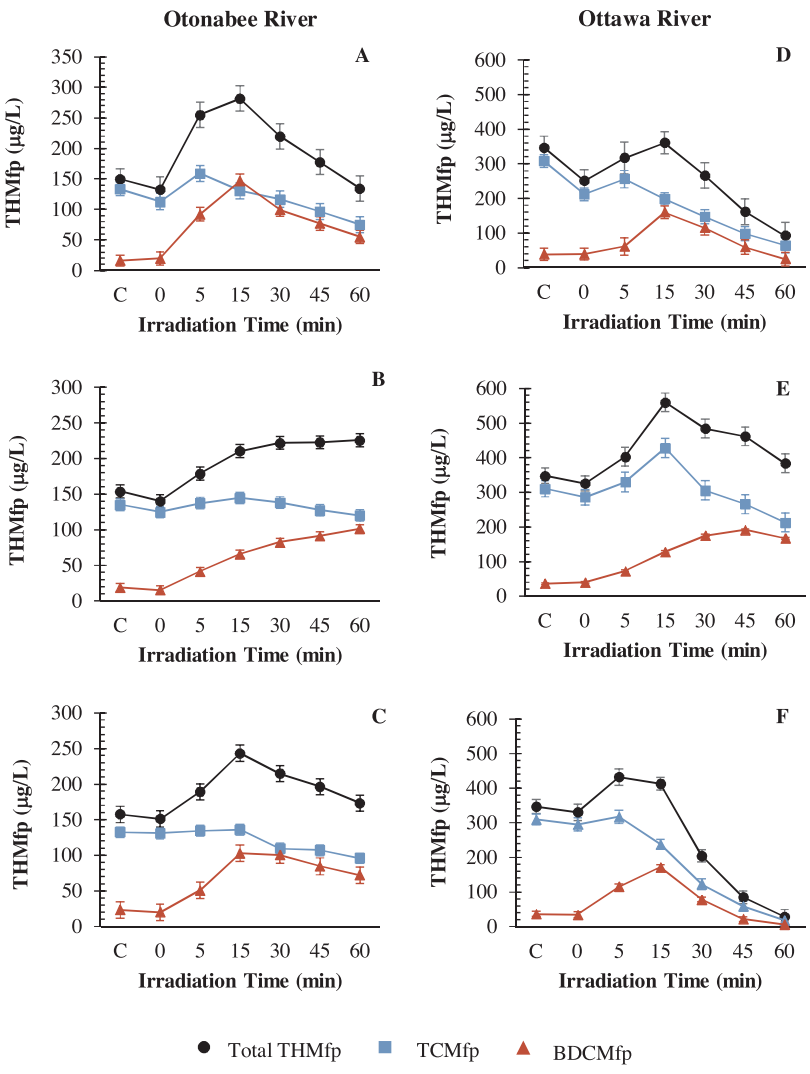

Fig. 6. Reduction in the formation of trihalomethanes in two water matrices after treatment by (A) P25 in OTB water, (B) NB 550 in OTB water, (C) NB 700 in OTB water, (D) P25 in OTW water, (E) NB 550 in OTW water, (F) NB 700 in OTW water. Error bars represent the 95% confidence interval of the mean.

upon chlorination. In this study, only dichloroacetic acid (DCAA) and trichloroacetic acid (TCAA) were formed at levels above 5 µg/L upon chlorination. For all three TiO_2 nanomaterials, the overall HAAfp of both water sources decreased slightly during the dark adsorption step, increased at short irradiation times, and eventually decreased as irradiation time increased. There were, however, important differences in HAA precursor removal between the two water matrices and the three materials.

In the OTB experiments (Fig. 7A–C), P25 reduced the overall HAAfp of the water from 74.9 ± 9.0 µg/L to 45.5 ± 6.4 µg/L after 60 min of irradiation. When NB 550 and NB 700 were used, the overall HAAfp of the water after 60 min of irradiation was equal to that of the untreated raw water. In both cases, the overall HAAfp of the water increased between 0 and 15 min of irradiation but decreased thereafter. The increases in overall HAAfp can be attributed to the initial increase in both DCAAfp and TCAAfp between 0 and 15 min. This was followed by a gradual reduction in TCAAfp over time as TCAA precursors were degraded by further treatment. TCAA precursors are more hydrophobic than DCAA precursors [47], and, as shown in earlier work [4], hydrophobic and aromatic NOM is preferentially degraded by TiO_2 photocatalysis. Other researchers have also observed preferential removal of TCAA precursors over DCAA precursors in AOP systems. These include Toor and Mohseni [48]; who linked increased DCAAfp in water treated with UV/H_2O_2 to the formation of aldehydes, known DCAA precursors, as a result of the partial degradation of NOM; and Bond et al. [49], who attributed the increase in DCAAfp to the transformation of hydrophilic NOM compounds (amino acids) into DCAA precursors via oxidation.

Photocatalytic degradation of HAA precursors occurred more readily in the OTW water matrix (Fig. 7D–F), particularly when NB 700 was employed as the photocatalyst. After 60 min of irradiation the HAAfp of the water treated with NB 700 was reduced from 112.9 ± 7.1 µg/L to 12.1 ± 7.1 µg/L. P25 was nearly as effective as NB 700 in this water matrix, reducing the HAAfp of the water from 110.4 ± 12.5 µg/L to 30.1 ± 12.5 µg/L after 60 min of irradiation. In both cases, the DCAAfp of the water increased at shorter irradiation times before decreasing at longer irradiation times. TCAAfp reduction occurred more quickly than DCAAfp reduction, and for both P25 and NB 700 the TCAAfp of the water was reduced to below the detection limit after 60 min of irradiation, indicating that the photocatalytic treatment was particularly effective for the removal of TCAA precursors.

The effect of the treatment on the formation of individual HAA species was not only nanomaterial specific but also water matrix specific. In the experiments conducted with OTW water, all three nanomaterials initially increased the amount of DCAA and TCAA precursors in the water upon irradiation but eventually began to degrade them, resulting in nearly concurrent reduction of DCAAfp and TCAAfp at longer irradiation times. When P25 and NB 700 were added to the OTB water and irradiated DCAAfp initially increased or remained constant but this was not followed by the eventual decrease observed in the OTW experiments. These results suggest that the two water matrices contain different types of DCAA precursors or that the degradation of DCAA

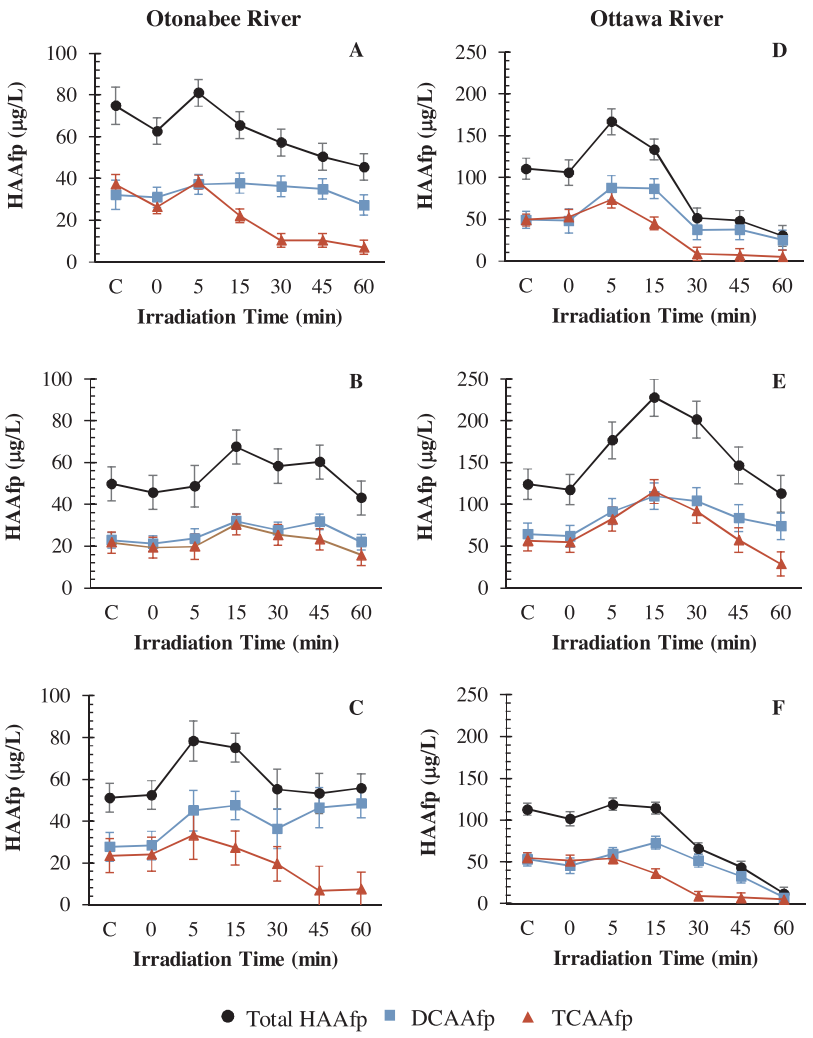

Fig. 7. Reduction in the formation of haloacetic acids in two water matrices after treatment by (A) P25 in OTB water, (B) NB 550 in OTB water, (C) NB 700 in OTB water, (D) P25 in OTW water, (E) NB 550 in OTW water, (F) NB 700 in OTW water. Error bars represent the 95% confidence interval of the mean.

precursors was in some way inhibited in the OTB water matrix. As was observed previously for THMfp, NB 700 was more strongly impacted by the presence of hydroxyl radical scavengers such as bicarbonate (alkalinity) than the other two nanomaterials. This may be because NOM oxidation by UV/TiO_2 treatment with this material proceeded primarily via hydroxyl radical mediated reactions, which were more likely to be inhibited in the higher alkalinity water matrix (OTB) than in the lower alkalinity water matrix (OTW).

With the exception of P25 in OTB water, the HAAfp of the adsorption only samples were statistically indistinguishable from the raw water controls at the 95% confidence level, an indication that none of the nanomaterials used in this study were reliably able to remove HAA precursors via adsorption alone at this dose of TiO_2. This is in line with previous studies conducted with P25 in this water source [4].

3.5. Correlations between DOC, UV254, and DBPfp

DOC and UV254 removal are widely used to predict reductions in THMfp because they are simple, inexpensive surrogate parameters that have been correlated to DBPfp in conventional water treatment systems. Pearson correlation coefficients between DOC, UV254, THMfp, and HAAfp were calculated at the 95% confidence level and are summarized in Table S.2 in the Supplementary material. DOC removal was significantly correlated to THMfp and HAAfp reduction in the tests conducted with P25 and NB 700 in OTW water, indicating that in this source water DOC was an acceptable surrogate for THMfp and HAAfp changes related to the photocatalytic degradation of NOM by these highly photoactive TiO_2 nanomaterials. DOC was not significantly correlated to THMfp or HAAfp reduction in any of the other experiments. UV254 was significantly correlated to HAAfp reduction by P25 and NB 700 in the OTW water and to THMfp reduction by NB 700 in OTW water. The lack of a consistent relationship between the reduction of THMfp and HAAfp and the removal of common NOM surrogates underscores the fact that the removal of simple indicator parameters cannot always be used to predict the removal or reduction of complex parameters such as THMfp and HAAfp.

4. Summary and conclusions

Two TiO_2 LENs were characterized based on size, surface characteristics, and crystal structure and compared to standard commercial P25 TiO_2 nanomaterials in terms of their ability to degrade disinfection byproduct precursors in natural water. The filterability of the three materials was also evaluated. Both LENs were more quickly removed from purified water and natural water via filtration than commercial P25 nanoparticles, likely because their larger size prevented them from becoming stuck in the filter pores.

Although all three materials reduced DOC and UV254 even at short irradiation times, the THMfp and HAAfp of the treated water initially increased upon irradiation with UVA LED light irrespective of the material or water source used. After 60 min of irradiation, one of the LENs, NB 700, removed more than 90% of the THMfp and HAAfp from one of the water sources. The types of DBP precursors present in the treated water changed over time as the original NOM compounds were

photocatalytically degraded from the larger, more aromatic precursors of DBPs such as TCM and TCAA, to smaller, less aromatic precursors of DBPs such as BDCM and DCAA.

The EEO required to degrade DOC and THM precursors varied by material and water source and in some cases was comparable to EEO values for UV/H_2O_2 reported by others. The EEO results suggest that a system incorporating NB 700 and UVA LED irradiation may be as energy efficient as UV/H_2O_2 in some water matrices, though this should be confirmed in parallel experiments under a wider range of experimental conditions.

DOC and UV254 removals were not always well correlated to THMfp and HAAfp removal. The results of this study should serve as a caution to researchers looking to quickly evaluate the photocatalytic properties of novel TiO_2 materials to determine whether they can be incorporated into drinking water treatment processes.

Throughout this study, the characteristics of the water matrix that impact radical scavenging (e.g. alkalinity) and particle agglomeration (e.g. hardness ions) had important effects on the removal of DBP precursors via degradation and adsorption by the TiO_2 nanomaterials. This finding highlights the need for comprehensive and site-specific evaluation of new engineered nanomaterials and other advanced oxidation processes ahead of their implementation for drinking water treatment.

Funding

Funding for this study was provided through Canada's Natural Sciences and Engineering Research Council's Strategic Project Grant program [STPGP 430654-12] and Canada Graduate Scholarship program as well as through the Ontario Graduate Scholarship program.

Acknowledgements

The authors would like to acknowledge the assistance of Kennedy Santos, Jim Wang, and Chuqiao (Kaya) Yuan in the laboratory.

Appendix A. Supplementary data

Supplementary data associated with this article can be found, in the online version, at https://doi.org/10.1016/j.jece.2017.11.068.

References

[1] S.W. Krasner, The formation and control of emerging disinfection by-products of health concern, Philos. Trans. R. Soc. A Math. Phys. Eng. Sci. 367 (2009) 4077–4095, http://dx.doi.org/10.1098/rsta.2009.0108.
[2] D. Zheng, R.C. Andrews, S.A. Andrews, L. Taylor-Edmonds, Effects of coagulation on the removal of natural organic matter, genotoxicity, and precursors to halogenated furanones, Water Res. 70 (2015) 118–129, http://dx.doi.org/10.1016/j.watres.2014.11.039.
[3] S. Liu, M. Lim, R. Fabris, C. Chow, M. Drikas, R. Amal, TiO2 photocatalysis of natural organic matter in surface water: impact on trihalomethane and haloacetic acid formation potential, Environ. Sci. Technol. 42 (2008) 6218–6223 http://www.ncbi.nlm.nih.gov/pubmed/18767690.
[4] S.L. Gora, S.A. Andrews, Adsorption of natural organic matter and disinfection byproduct precursors from surface water on TiO2 Nanoparticles: pH effects, isotherm modelling and implications for using TiO2 for drinking water treatment, Chemosphere 174 (2017) 363–370, http://dx.doi.org/10.1016/j.chemosphere.2017.01.125.
[5] F.C. Kent, K.R. Montreuil, R.M. Brookman, R. Sanderson, J.R. Dahn, G. a Gagnon, Photocatalytic oxidation of DBP precursors using UV with suspended and fixed TiO2, Water Res. 45 (2011) 6173–6180, http://dx.doi.org/10.1016/j.watres.2011.09.013.
[6] X. Huang, M. Leal, Q. Li, Degradation of natural organic matter by TiO2 photocatalytic oxidation and its effect on fouling of low-pressure membranes, Water Res. 42 (2008) 1142–1150, http://dx.doi.org/10.1016/j.watres.2007.08.030.
[7] K.K. Philippe, C. Hans, J. MacAdam, B. Jefferson, J. Hart, S.A. Parsons, Photocatalytic oxidation of natural organic matter surrogates and the impact on trihalomethane formation potential, Chemosphere 81 (2010) 1509–1516, http://dx.doi.org/10.1016/j.chemosphere.2010.08.035.
[8] S. Liu, M. Lim, R. Fabris, C. Chow, M. Drikas, R. Amal, Comparison of photocatalytic degradation of natural organic matter in two Australian surface waters using multiple analytical techniques, Org. Geochem. 41 (2010) 124–129, http://dx.doi.org/10.1016/j.orggeochem.2009.08.008.
[9] O. Autin, J. Hart, P. Jarvis, J. MacAdam, S.A. Parsons, B. Jefferson, The impact of background organic matter and alkalinity on the degradation of the pesticide metaldehyde by two advanced oxidation processes: UV/H2O2 and UV/TiO2, Water Res. 47 (2013) 2041–2049, http://dx.doi.org/10.1016/j.watres.2013.01.022.
[10] C.H. Liao, S.F. Kang, F.A. Wu, Hydroxyl radical scavenging role of chloride and bicarbonate ions in the H2O2/UV process, Chemosphere 44 (2001) 1193–1200, http://dx.doi.org/10.1016/S0045-6535(00)00278-2.
[11] M. Abdullah, G.K.-C. Low, R.W. Matthews, Effects of common inorganic anions on rates of photocatalytic oxidation of organic carbon over illuminated titanium dioxide, J. Phys. Chem. 94 (1990) 6820–6825, http://dx.doi.org/10.1021/j100380a051.
[12] H.Y. Chen, O. Zahraa, M. Bouchy, Inhibition of the adsorption and photocatalytic degradation of an organic contaminant in an aqueous suspension of TiO2 by inorganic ions, J. Photochem. Photobiol. A Chem. 108 (1997) 37–44, http://dx.doi.org/10.1016/S1010-6030(96)04411-5.
[13] E.M. Hotze, T. Phenrat, G.V. Lowry, Nanoparticle aggregation: challenges to understanding transport and reactivity in the environment, J. Environ. Qual. 39 (1909) (2010), http://dx.doi.org/10.2134/jeq2009.0462.
[14] W. Liu, W. Sun, A.G.L. Borthwick, J. Ni, Comparison on aggregation and sedimentation of titanium dioxide, titanate nanotubes and titanate nanotubes-TiO2: Influence of pH, ionic strength and natural organic matter, Colloids Surf. A Physicochem. Eng. Aspects 434 (2013) 319–328, http://dx.doi.org/10.1016/j.colsurfa.2013.05.010.
[15] Y. Zhang, Y. Chen, P. Westerhoff, J. Crittenden, Impact of natural organic matter and divalent cations on the stability of aqueous nanoparticles, Water Res. 43 (2009) 4249–4257, http://dx.doi.org/10.1016/j.watres.2009.06.005.
[16] M. Erhayem, M. Sohn, Stability studies for titanium dioxide nanoparticles upon adsorption of Suwannee River humic and fulvic acids and natural organic matter, Sci. Total Environ. 468–469 (2014) 249–257, http://dx.doi.org/10.1016/j.scitotenv.2013.08.038.
[17] D. Chen, A.K. Ray, Removal of toxic metal ions from wastewater by semiconductor photocatalysis, Chem. Eng. Sci. 56 (2001) 1561–1570, http://dx.doi.org/10.1016/S0009-2509(00)00383-3.
[18] E.C. Butler, A.P. Davis, Photocatalytic oxidation in aqueous titanium dioxide suspensions: the influence of dissolved transition metals, J. Photochem. Photobiol. A Chem. 70 (1993) 273–283, http://dx.doi.org/10.1016/1010-6030(93)85053-B.
[19] M.I. Franch, J.A. Ayllón, J. Peral, X. Domènech, Enhanced photocatalytic degradation of maleic acid by Fe(III) adsorption onto the TiO2 surface, Catal. Today 101 (2005) 245–252, http://dx.doi.org/10.1016/j.cattod.2005.03.007.
[20] M. Ng, E.T. Kho, S. Liu, M. Lim, R. Amal, Highly adsorptive and regenerative magnetic TiO2 for natural organic matter (NOM) removal in water, Chem. Eng. J. 246 (2014) 196–203, http://dx.doi.org/10.1016/j.cej.2014.02.015.
[21] S. Liu, M. Lim, R. Amal, TiO2-coated natural zeolite: rapid humic acid adsorption and effective photocatalytic regeneration, Chem. Eng. Sci. 105 (2014) 46–52, http://dx.doi.org/10.1016/j.ces.2013.10.041.
[22] D.V. Bavykin, K.E. Redmond, B.P. Nias, A.N. Kulak, F.C. Walsh, The effect of ionic charge on the adsorption of organic dyes onto titanate nanotubes, Aust. J. Chem. 63 (2010) 270–275, http://dx.doi.org/10.1071/CH09326.
[23] X. Zhang, J.H. Pan, A.J. Du, W. Fu, D.D. Sun, J.O. Leckie, Combination of one-dimensional TiO2 nanowire photocatalytic oxidation with microfiltration for water treatment, Water Res. 43 (2009) 1179–1186, http://dx.doi.org/10.1016/j.watres.2008.12.021.
[24] S. Gora, R. Liang, Y.N. Zhou, S. Andrews, Settleable engineered titanium dioxide nanomaterials for the removal of natural organic matter from drinking water, Chem. Eng. J. 334 (2018) 638–649, http://dx.doi.org/10.1016/j.cej.2017.10.058.
[25] Z.-Y. Yuan, B.-L. Su, Titanium oxide nanotubes, nanofibers and nanowires, Colloids Surf. A Physicochem. Eng. Aspects 241 (2004) 173–183, http://dx.doi.org/10.1016/j.colsurfa.2004.04.030.
[26] C.L. Wong, Y.N. Tan, A.R. Mohamed, A review on the formation of titania nanotube photocatalysts by hydrothermal treatment, J. Environ. Manag. 92 (2011) 1669–1680, http://dx.doi.org/10.1016/j.jenvman.2011.03.006.
[27] M. Qamar, C.R. Yoon, H.J. Oh, N.H. Lee, K. Park, D.H. Kim, K.S. Lee, W.J. Lee, S.J. Kim, Preparation and photocatalytic activity of nanotubes obtained from titanium dioxide, Catal. Today 131 (2008) 3–14, http://dx.doi.org/10.1016/j.cattod.2007.10.015.
[28] Z. Zheng, H. Liu, J. Ye, J. Zhao, E.R. Waclawik, H. Zhu, Structure and contribution to photocatalytic activity of the interfaces in nanofibers with mixed anatase and TiO2(B) phases, J. Mol. Catal. A Chem. 316 (2009) 75–82, http://dx.doi.org/10.1016/j.molcata.2009.10.002.
[29] S. Ali, H. Granbohm, Y. Ge, V.K. Singh, F. Nilsén, S.P. Hannula, Crystal structure and photocatalytic properties of titanate nanotubes prepared by chemical processing and subsequent annealing, J. Mater. Sci. 51 (2016) 7322–7335, http://dx.doi.org/10.1007/s10853-016-0014-5.
[30] P. Mwaanga, E.R. Carraway, M.A. Schlautman, Preferential sorption of some natural organic matter fractions to titanium dioxide nanoparticles: influence of pH and ionic strength, Environ. Monit. Assess. 186 (2014) 8833–8844, http://dx.doi.org/10.1007/s10661-014-4047-4.
[31] M. Erhayem, M. Sohn, Effect of humic acid source on humic acid adsorption onto titanium dioxide nanoparticles, Sci. Total Environ. 470–471 (2014) 92–98, http://dx.doi.org/10.1016/j.scitotenv.2013.09.063.
[32] R.a. French, A.R. Jacobson, B. Kim, S.L. Isley, R.L.E.E. Penn, P.C. Baveye, Influence of ionic strength, pH, andcation valence on aggregation kinetics of titanium dioxide nanoparticles, Environ. Sci. Technol. 43 (2009) 1354–1359, http://dx.doi.org/10.1021/es802628n.
[33] F. Loosli, L. Vitorazi, J.-F. Berret, S. Stoll, Towards a better understanding on agglomeration mechanisms and thermodynamic properties of TiO2 nanoparticles

interacting with natural organic matter, Water Res. 80 (2015) 139–148, http://dx.doi.org/10.1016/j.watres.2015.05.009.
[34] L. Li, M. Sillanpää, M. Risto, Influences of water properties on the aggregation and deposition of engineered titanium dioxide nanoparticles in natural waters, Environ. Pollut. 219 (2016) 132–138, http://dx.doi.org/10.1016/j.envpol.2016.09.080.
[35] Ministry of the Environment and Climate Change, Drinking Water Surveillance Program, Drink. Water Surveill. Progr. (2013).
[36] J.R. Bolton, K.G. Linden, M. Asce, Standardization of methods for fluence: UV dose determination in bench-Scale UV experiments, J. Environ. Eng. 129 (2003) 209–215.
[37] B.T. Kasuga, M. Hiramatsu, A. Hoson, T. Sekino, K. Niihara, Titania nanotubes prepared by chemical processing, Adv. Mater. 567 (1999) 1307–1311.
[38] M. Klinger, A. Jäger, Crystallographic tool box (CrysTBox): Automated tools for transmission electron microscopists and crystallographers, J. Appl. Crystallogr. 48 (2015) 2012–2018, http://dx.doi.org/10.1107/S1600576715017252.
[39] M.J. Arlos, R. Liang, M.M. Hatat-Fraile, L.M. Bragg, N.Y. Zhou, M.R. Servos, S.A. Andrews, Photocatalytic decomposition of selected estrogens and their estrogenic activity by UV-LED irradiated TiO2 immobilized on porous titanium sheets via thermal-chemical oxidation, J. Hazard. Mater. 318 (2016) 541–550, http://dx.doi.org/10.1016/j.jhazmat.2016.07.048.
[40] A. Turolla, A. Piazzoli, J. Farner Budarz, M.R. Wiesner, M. Antonelli, Experimental measurement and modelling of reactive species generation in TiO2 nanoparticle photocatalysis, Chem. Eng. J. 271 (2015) 260–268, http://dx.doi.org/10.1016/j.cej.2015.03.004.
[41] K. Ishibashi, A. Fujishima, T. Watanabe, K. Hashimoto, Quantum yields of active oxidative species formed on TiO2 photocatalyst, J. Photochem. Photobiol. A Chem. 134 (2000) 139–142, http://dx.doi.org/10.1016/S1010-6030(00)00264-1.
[42] American Public Health Association, American Water Works Association, Water Environment Federation,, Standard Methods for the Examination of Water and Wastewater, 21st ed., APHA-AWWA-WEF, Washington, D.C, 2005.
[43] J.C. Crittenden, R.R. Trussell, D.W. Hand, K.J. Howe, G. Tchobanoglous, MWH's Water Treatment: Principles and Design, 3rd Edition, John Wiley and Sons, 2012.
[44] R.S. Summers, S.M. Hooper, H.M. Shukairy, G. Solarik, R.S. Summers, S.M. Hooper, D. Owen, Assessing DBP yield: uniform formation conditions reviewed work (s), Am. Water Works Assoc. 88 (6) (1996) 80–93 DBPs (JUNE 1996). Published by: American Water Works Association Stable URL: http://www.jstor.org/shttp://www.jstor.org/s.
[45] H.Y. Yen, L.S. Yen, Reducing THMFP by H\n 2\n O\n 2\n/UV oxidation for humic acid of small molecular weight, Environ. Technol. 36 (2014) 417–423, http://dx.doi.org/10.1080/09593330.2014.951075.
[46] D. Gerrity, B. Mayer, H. Ryu, J. Crittenden, M. Abbaszadegan, A comparison of pilot-scale photocatalysis and enhanced coagulation for disinfection byproduct mitigation, Water Res. 43 (2009) 1597–1610, http://dx.doi.org/10.1016/j.watres.2009.01.010.
[47] L. Liang, P.C. Singer, Factors influencing the formation and relative distribution of haloacetic acids and trihalomethanes in drinking water, Environ. Sci. Technol. 37 (2003) 2920–2928, http://dx.doi.org/10.1021/es026230q.
[48] R. Toor, M. Mohseni, UV-H2O2 based AOP and its integration with biological activated carbon treatment for DBP reduction in drinking water, Chemosphere 66 (2007) 2087–2095, http://dx.doi.org/10.1016/j.chemosphere.2006.09.043.
[49] T. Bond, E.H. Goslan, B. Jefferson, F. Roddick, L. Fan, S.A. Parsons, Chemical and biological oxidation of NOM surrogates and effect on HAA formation, Water Res. 43 (2009) 2615–2622, http://dx.doi.org/10.1016/j.watres.2009.03.036.